Rydberg–valence interactions in $CH_2Cl \rightarrow CH_2 + Cl$ photodissociation: Dependence of absorption probability on ground state vibrational excitation

Sergey V. Levchenko, Andrei V. Demyanenko, Vladimir L. Dribinski, Aaron B. Potter, Hanna Reisler, and Anna I. Krylov
Department of Chemistry, University of Southern California, Los Angeles, California 90089-0482

(Received 22 January 2003; accepted 25 February 2003)

A strong enhancement of absorption to the lowest $^2A_1$ state is observed for vibrationally excited chloromethyl radicals. It is demonstrated that this enhancement is due to a significant increase in both electronic and vibrational Franck–Condon factors. Electronic structure calculations of potential energy surfaces (PESs) and transition dipole moments for the ground and the two lowest excited states of A_1 symmetry, the $1\,^2A_1$ valence and $2\,^2A_1$ Rydberg states, reveal the origin of this effect. The shelflike shape of the $1\,^2A_1$ PES in the Franck–Condon region and the strong dependence of the electronic transition dipole moment on C–Cl distance are responsible for the enhancement. Analysis of the shape of the electron density distribution demonstrates that Rydberg–valence interaction in the two lowest excited states causes the changes in the shape of PESs and transition dipoles with C–Cl distance. © *2003 American Institute of Physics.* [DOI: 10.1063/1.1568076]

I. INTRODUCTION

The interest in the chloromethyl radical originates in its possible role in atmospheric reactions.[1,2] For example, CH_2Cl and other halogen-substituted methyl radicals are intermediates in the photodecomposition and oxidation reactions of halogenated hydrocarbons that represent an important source of halogen atoms in the atmosphere.[1,2] Moreover, photodissociation of CH_2Cl and other small polyatomic molecules provides an ideal opportunity for the study of molecular dynamics at a detailed state-to-state level.[3]

Halogen-substituted small radicals exhibit several general phenomena, such as additional bonding due to the interaction of the unpaired electron with the lone pairs of the halogen,[4] unusually large ($\pm 100\%$) out-of-plane (OPLA) mode anharmonicities caused by the unpaired electron,[5] and Rydberg–valence interactions in excited states.

Recently, the photodissociation of CH_2Cl was investigated experimentally by Reisler and co-workers.[6,7] Using the ion imaging technique, they concluded that $Cl + CH_2$ was the main channel in the wavelength region 312–214 nm. They found a broad maximum in product yield at ~ 250 nm (4.96 eV) associated with a perpendicular electronic transition, in excellent agreement with the calculated 4.92 eV value for the vertical $1\,^2A_1 \leftarrow X\,^2B_1$ excitation.[4] The valence character of the $1\,^2A_1$ state[4] rationalizes the observed fast dissociation.[6] With shorter excitation wavelengths (240–214 nm), products deriving from a parallel transition were also detected.[6] *Ab initio* calculations[4] identified the upper state as $2\,^2B_1$ resulting from a $\pi^*_{CCl} \leftarrow \pi_{CCl}$ promotion of the unpaired electron. The large absorption cross section for this transition[4,8] is responsible for its contributions to the photodissociation at energies considerably lower than the vertical excitation energy of 6.33 eV (theoretical estimate,[4] in agreement with the experimental value of 6.2 eV[8]).

The focus of the present work is the photodissociation from the $1\,^2A_1$ excited state. For this state, it was observed that despite efficient vibrational and rotational cooling of CH_2Cl by carrier gases in supersonic expansion, a large fraction of the dissociation products appeared with total energies exceeding the energy available to vibrationally *unexcited* radicals after photon absorption.[6] Quantitatively, the relative product yields from vibrationally excited radicals are greater than predicted based solely on the thermal ''hot band'' population. This suggests a significant enhancement in absorption probabilities for vibrationally excited radicals. To explain this finding, we calculated potential energy surfaces (PESs) and transition dipole moments along the C–Cl bond-breaking coordinate for the ground and the $1\,^2A_1$ and $2\,^2A_1$ excited states. We find that the shelflike shape of the $1\,^2A_1$ PES in the Franck–Condon region and the strong dependence of the electronic transition dipole upon the C–Cl distance are responsible for the enhancement. We conclude that it is the Rydberg–valence interaction between the two lowest excited states that causes the changes in the shape of PESs and transition dipoles with C–Cl distance. Such Rydberg–valence interactions are common in bond breaking,[9] especially in radicals, which often have low-lying valence and Rydberg states.[4]

The equilibrium properties of the two lowest $^2A_1$ states are also characterized. The shapes of the PESs and the changes in vibrational frequencies are explained in terms of a molecular orbital picture developed in our previous work.[4]

The structure of the paper is as follows. Section II presents the experimental evidence for the enhancement in product intensities from ''hot bands,'' and demonstrates that it can only be explained by a considerable increase in Franck–Condon factors for vibrationally excited CH_2Cl. In Sec. III, results of *ab initio* calculations are summarized and discussed. Section III A describes technical details of the calculations; Sec. III B presents our analysis of the equilibrium structures, vibrational frequencies, and PESs of the ground and the two lowest excited states of CH_2Cl; and Sec. III C

 © 2003 American Institute of Physics

Downloaded 14 Jul 2010 to 128.125.205.65. Redistribution subject to AIP license or copyright; see http://jcp.aip.org/jcp/copyright.jsp

discusses the shapes of the PESs in terms of Rydberg–valence interaction. Based on these results, Sec. IV explains the observed enhancement from ''hot bands.'' Our final remarks and conclusions are given in Sec. V.

II. EXPERIMENTAL RESULTS

Experimental results on the photodissociation of CH_2Cl following excitation at selected wavelengths in the region 214–312 nm were reported elsewhere.[6,7] The CH_2Cl radical was produced in a molecular beam by using pulsed pyrolysis. The gas mixture, 0.5–1 % of CH_2ClI in 2 atm of He, Ar, or different mixtures of CF_4:He, was expanded through a pulsed supersonic nozzle with an attached SiC tube.[10] The tube was heated to a temperature of $T \approx 1800$ K, which resulted in the fission of I atoms from CH_2ClI with an efficiency greater than 50%. After supersonic expansion, the radicals were photodissociated with laser radiation. The photofragments were detected by resonance enhanced multiphoton ionization (REMPI), and their velocity and angular distributions were determined using the velocity map ion imaging technique, as described before.[11,12]

Cl and CH_2 fragments are the major products throughout the excitation wavelength region 214–312 nm:

$$CH_2Cl \rightarrow Cl + CH_2, \quad \Delta H = 391 \pm 5 \ \text{kJ mol}^{-1}. \tag{1}$$

In the region 247–312 nm CH_2 ($X\,^3B_1$) and Cl ($^2P_{1/2,3/2}$) products derive predominantly from dissociation via the perpendicular ($\beta = -0.7$) electronic transition $1\,^2A_1 \leftarrow X\,^2B_1$. At wavelengths shorter than 240 nm, the Cl ($^2P_{1/2,3/2}$) products exhibit angular distributions that are characteristic of a parallel transition ($2\,^2B_1 \leftarrow X\,^2B_1$; $\beta = 1.2$), and $CH_2(\tilde{a}\,^1A_1)$ is the main co-fragment.

The measured velocity distributions were converted into translational energy distributions of the products (see Fig. 1). The widths of the energy distributions for Cl correspond to a range of internal excitations in the CH_2 co-fragment. The maximum allowed translational energy for ground state reactants, $E_t^{\max}$ is given by

$$E_t^{\max} = h\nu - D_0, \tag{2}$$

where D_0 is the dissociation threshold. The complete energy balance for CH_2Cl dissociation is given by

$$E_{\text{int}}(CH_2Cl) + h\nu = D_0 + E_t + E_{\text{int}}(CH_2) + E_{\text{int}}(Cl), \tag{3}$$

where $h\nu$ is the photon energy, D_0 is the dissociation threshold of the CH_2Cl radical, and $E_{\text{int}}(CH_2Cl)$, $E_{\text{int}}(CH_2)$, and $E_{\text{int}}(Cl)$ are the internal energies (rotational, vibrational, and electronic) of the respective reactant and fragments. The value of $D_0 = 391 \pm 5$ kJ/mol ($32\,690 \pm 420$ cm^{-1}), was derived from the enthalpies of formation of CH_2Cl, CH_2, and Cl.[13–20] In experiments carried out with He carrier gas, we found that in the excitation range 214–240 nm (parallel transition) the measured highest translational energy is close to $E_t^{\max}$, while for photolysis via the perpendicular transition (247–312 nm) large fractions of the products have translational energies exceeding $E_t^{\max}$ [see Fig. 1(a)].

Based on previous work,[21,22] effective rotational cooling of CH_2Cl radicals is expected in supersonic expansion combined with the pyrolysis source, but He is not efficient in relaxing vibrational excitations. Typically in supersonic cooling $T_{\text{vib}} = 30–60$ K and $T_{\text{rot}} = 2–10$ K are achieved. Considering the high initial temperature of the radical produced in the 1800 K pyrolysis one may assume a somewhat higher final vibrational temperature of the radical (few hundreds instead of few tens of degrees). Thus, the high energy tails of the observed product distributions can be attributed to dissociation of vibrationally excited (''hot'') CH_2Cl radicals. Another possible source of fragments with excess kinetic energy, two-photon dissociation of CH_2Cl, was ruled out before.[6]

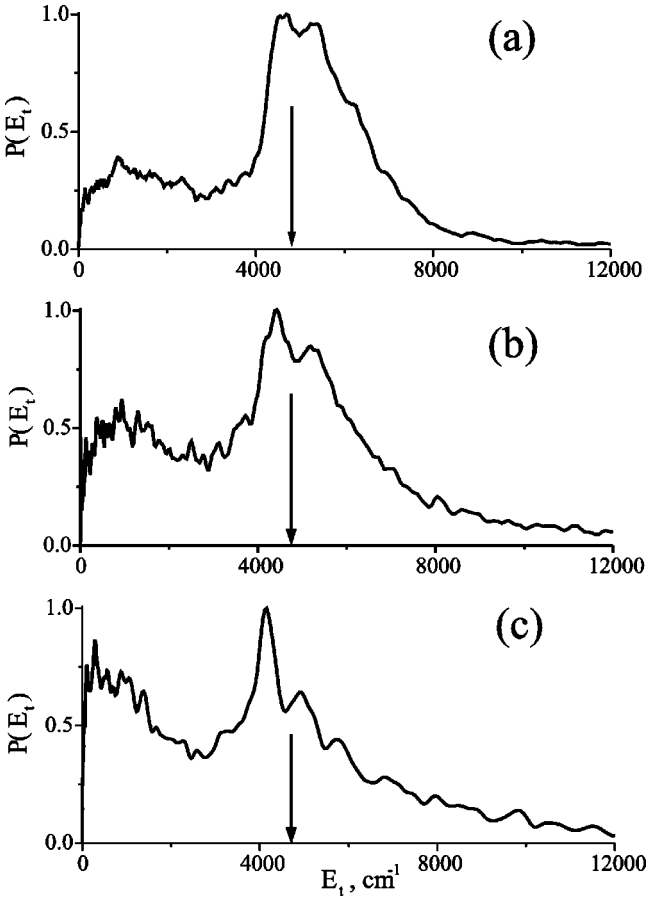

FIG. 1. CH_2Cl photodissociation at 266 nm (37 594 cm^{-1}) using (a) He, (b) CF_4:He (1:7), and (c) Ar carrier gases. Cl($^2P_{3/2}$) signals are plotted as a function of the total c.m. photofragment translational energy, E_t. The arrows indicate the maximum translational energy allowed for dissociation from the ground vibrational state to Cl($^2P_{3/2}$) + $CH_2(X\,^3B_1)$.

In order to confirm that products with kinetic energy in excess of $E_t^{\max}$ result from dissociation of vibrationally excited radicals, we carried out experiments with Ar and He/CF_4 mixtures as carrier gases. Figure 1(c) shows the energy distribution of Cl($^2P_{3/2}$) obtained from the dissociation of CH_2Cl at 266 nm in Ar carrier gas and detected at 235.337 nm. Similar results were obtained with 247 nm photolysis, though the ''hot band'' component was substantially smaller. Compared with the He results [Fig. 1(a)], two main differences are observed. First, the Cl translational energy distribution becomes narrower with the largest peak at high energies corresponding to the dissociation of vibrationally ''cold'' CH_2Cl. Second, a bandlike structure is discernible

Downloaded 14 Jul 2010 to 128.125.205.65. Redistribution subject to AIP license or copyright; see http://jcp.aip.org/jcp/copyright.jsp

TABLE I. Ground and excited state geometries of CH_2Cl radical.

	Symm.	r_{CH}, Å	r_{CCl}, Å	α_{HCH}	Θ[a]	Total energy, hartrees
$X\ ^2B_1$[b]	C_{2v}	1.076	1.691	124.17	180	−499.007 704
$1\ ^2A_1$[c]	C_{2v}	1.092	2.095	121.98	180	−498.843 600
$X\ ^1A_1 CH_2Cl^+$[b]	C_{2v}	1.088	1.590	121.91	180	−498.692 604

[a]Dihedral H–C–Cl–H angle.
[b]CCSD(T)/6-311(+,+)G($3df$,$3pd$). The cation structure approximates the structure of the Rydberg $2\ ^2A_1$ state.
[c]EOM–CCSD/6-311(+,+)G($3df$,$3pd$).

with $\sim 800\ cm^{-1}$ separation between bands, close to the frequency of the C–Cl stretch in CH_2Cl (see Table II). The vibrational relaxation in CH_2Cl can be enhanced by using molecular carrier gases, and therefore various mixtures of CF_4:He were also used [Fig. 1(b)]. Depending on the CF_4:He ratio, the results range between pure He and Ar.

However, a high vibrational temperature in the ground electronic state of the radical cannot alone explain the large fraction of ''hot band'' component in the translational energy distributions at 247–312 nm. This follows directly from comparison with the results obtained with 214–240 nm photolysis (parallel-type excitation), where the maximum translational energy of the products does not exceed significantly E_t^{max}, and does not depend on carrier gas. Also, at 247–312 nm the effect of the carrier gas depends on the photolysis wavelength. We find that while at $\lambda \geqslant 280$ nm most of the CH_2 and Cl signals derive from ''hot band'' excitation, at 266 nm the contribution of fragments with translational energies exceeding E_t^{max} is smaller, and this fraction decreases further at 247 nm.

The above observations and analysis indicate that for the perpendicular transition, the fraction of fragments with translational energies greater than E_t^{max} is larger than expected based on a thermal vibrational population and equal excitation efficiency for excited and unexcited radicals. A large increase in the Franck–Condon factors for ''hot band'' excitation must also be taken into account. This implies that the ground and excited electronic state geometries must be rather different. The lowest vibrational frequency in CH_2Cl is associated with the OPLA bend ($\sim 390\ cm^{-1}$).[23,24] This mode should give the largest contribution to the ''hot band'' populations, and its substantial cooling in Ar carrier gas is expected. However, even in Ar some of the Cl fragments have energies exceeding E_t^{max}, with bands separated by $\sim 800\ cm^{-1}$, i.e., the C–Cl stretch frequency in CH_2Cl. The persistence of the C–Cl vibrational structure in the translational energy distribution, even upon cooling in Ar, suggests a large geometrical change in the C–Cl coordinate between the ground and $1\ ^2A_1$ state. Therefore, *ab initio* calculations of the PES along this coordinate were carried out as described below.

III. ELECTRONIC STRUCTURE CALCULATIONS

A. Computational details

The ground state structures and harmonic frequencies of CH_2Cl and CH_2Cl^+ (which approximates the Rydberg states) are calculated by the CCSD(T)[25] method, using the ACES II electronic structure program.[26] The equilibrium structure and vibrational frequencies of the valence state are computed by the EOM–CCSD[27,28] method. Potential energy surfaces (PESs) along the C–Cl bond breaking coordinate of the ground and excited states are calculated by using the CCSD[29] and the EOM–CCSD[27,28] methods, respectively. Geometry optimizations and vibrational analysis are performed using the 6-311(+, +)G($3df$,$3pd$) basis set, derived from the polarized split-valence 6-311G(d,p) basis[30,31] by augmenting it by additional sets of polarization and diffuse functions.[32,33] For PESs, 6-311(3+, 3+)G($3df$, $3pd$) is employed.

The ground and excited states' PESs along the C–Cl coordinate are calculated with the C–H bond length and the H–C–H angle fixed at their ground state equilibrium values. In this study, we vary the C–Cl distance from 1.25 to 2.7 Å. Thus, the displacements from the ground state equilibrium C–Cl distance of 1.69 Å are small enough for the CCSD and EOM–CCSD results to be reliable. We calculate total energies, transition dipole moments, and average sizes of the electron density for the $X\ ^2B_1$ ground state and the two lowest $^2A_1$ excited states: the $1\ ^2A_1$ $\sigma^*_{CCl} \leftarrow \pi^*_{CCl}$ valence state and the $2\ ^2A_1$ $3s \leftarrow \pi^*_{CCl}$ Rydberg state. The calculated dipole strengths of the transitions and the PESs are then used to estimate vibrational overlaps and to calculate Franck–Condon factors.

B. Characterization of the two lowest $^2A_1$ excited states of CH_2Cl

Equilibrium structures and vibrational frequencies of the ground state, the valence $1\ ^2A_1$ excited state, and the CH_2Cl^+ cation are presented in Tables I and II. For a perfect Rydberg state (i.e., a highly excited electron orbiting a positively charged and structureless core), the optimized geometry should be close to that of the cation, and the CH_2Cl^+ calculations were performed to determine approximately the properties of the Rydberg states.[34]

The equilibrium structures and harmonic vibrational frequencies of the ground and $1\ ^1A_1$ valence excited state of CH_2Cl, and of CH_2Cl^+ (Table I) are in good agreement with the simple molecular orbital picture developed before.[4] We have found that the unpaired p electron on carbon interacts with the chlorine lone pair, which results in an additional $\frac{1}{2}\pi$ bond between C and Cl in the CH_2Cl ground state (this yields stronger C–Cl bonding in the radical relative to the saturated compound[24]). The lowest valence $1\ ^2A_1$ excited state is derived by promotion of the unpaired electron from the π^*_{CCl} antibonding orbital to the σ^*_{CCl} antibonding orbital (see Fig. 2 in Ref. 4). Therefore, in this state a full π bond

Downloaded 14 Jul 2010 to 128.125.205.65. Redistribution subject to AIP license or copyright; see http://jcp.aip.org/jcp/copyright.jsp

TABLE II. Calculated harmonic vibrational frequencies ω_e of the ground and excited states of CH_2Cl.

State	C–Cl stretch a_1	CH_2 scissors a_1	OPLA b_1	CH_2 rock b_2	CH_2 *s*-stretch a_1	CH_2 *a*-stretch b_2
$X\,^2B_1$[a]	868	1434	168[c]	1004	3179	3335
$1\,^2A_1$[b]	535	1256	1253	194	3026	3206
$X\,^1A_1CH_2Cl^+$[a]	1074	1492	1147	1056	3104	3249

[a]CCSD(T)/6-311(+,+)G(3*df*,3*pd*).
[b]EOM–CCSD/6-311(+,+)G(3*df*,3*pd*). The cation structure approximates the structure of the Rydberg $2\,^2A_1$ state.
[c]Due to large anharmonicity, the harmonic OPLA frequency is about twice lower than the anharmonic 01 transition. The theoretical value of ω_{01} is 422 cm^{-1} (Ref. 5).

exists, but the σ bond order decreases, and a planar structure with an elongated C–Cl bond relative to the ground state is preferred. Likewise, in $1\,^2A_1$ the C–Cl vibrational frequency is lower, while the OPLA vibrational frequency is considerably higher than in the ground state (due to the decrease in σ bond order and the increase in π bond order, respectively). The results presented in Tables I and II are consistent with this picture. Similar considerations explain the properties of the cation, which is derived by removing an electron from the π^*_{CCl} antibonding orbital. The full double C–Cl bond in the cation explains the C–Cl bond contraction relative to the ground state and the OPLA frequency increase up to 1147 cm^{-1}. This value approaches the OPLA frequency of the valence excited state (1253 cm^{-1}). For reference, the OPLA vibrational frequency of formaldehyde (CH_2O), a molecule with a full π_{CO} bond, is 1167 cm^{-1}.[14]

As seen in Table I, the difference between the C–H equilibrium bond lengths in the ground and the lowest excited state of the CH_2Cl radical is only 0.016 Å. The change in the H–C–H angle is also small (2.19°). This suggests that the minimum energy path for the C–Cl bond breaking reaction on the $1\,^2A_1$ PES is close to the pure C–Cl stretch (for C–Cl separations ~1.25–2.10 Å), and that the other degrees of freedom can be frozen. Thus, we calculate one-dimensional cuts of the PESs along the C–Cl stretch, with the values of the other two internal coordinates being fixed at the ground state equilibrium values. The resulting adiabatic potential energy curves are shown in Fig. 2.

The barrier on the $2\,^2A_1$ state curve is due to an avoided crossing of the Rydberg 3s state with the $9\,^2A_1$ valence state (which has been identified as a $\pi^*_{CCl} \leftarrow \sigma_{CCl}$ transition, and therefore is expected to be purely repulsive[4]). This is confirmed by the sharp drop in the size of the electron density for large C–Cl separations. Such behavior of Rydberg states in bond breaking reactions is general and was described by Gordon and co-workers (see Ref. 35 and references therein).

An interesting feature of the $1\,^2A_1$ curve shown in Fig. 2 is its shelflike shape in the vicinity of the ground state equilibrium geometry (i.e., in the active Franck–Condon region). Similar shapes of the excited state potentials were observed in alkali atom dimers,[36–39] where a double minimum is formed as a result of Rydberg–valence interaction.[36,39,40] In Sec. III C we will demonstrate that the shelf on the $1\,^2A_1$ PES indeed is a result of coupling between the valence and the 3*s* Rydberg states.

The calculated dependence of the electronic transition dipole strength on the C–Cl separation for the $1\,^2A_1 \leftarrow X\,^2B_1$ and $2\,^2A_1 \leftarrow X\,^2B_1$ transitions is shown in Fig. 3. Due to the Rydberg–valence interaction in the $1\,^2A_1$ and $2\,^2A_1$ states mentioned above, the dipole strength of the transition to the $1\,^2A_1$ state increases at shorter C–Cl distances (~1.6 Å) (see Sec. III C). As shown in Sec. IV, this behavior of the transition dipole moment contributes to the enhancement of the absorption probability for vibrationally excited CH_2Cl. The sharp rise in the $2\,^2A_1 \leftarrow X\,^2B_1$ transition dipole strength at $r_{CCl} < 1.6$ Å results from the increased $3p_z$ character at short C–Cl distances (see Sec. III C).

C. Rydberg–valence interactions in the lowest excited states of CH_2Cl

This section presents our analysis of the changes in the character of the wave functions for the two lowest adiabatic states along the C–Cl stretching coordinate. Avoided crossings due to Rydberg–valence interactions in closed-shell species were extensively characterized by Gordon and Caldwell,[35] and Salem.[9] Gordon's study[35,41] of saturated molecules (e.g., alkanes) demonstrates that their low-lying vertical excited states are Rydberg states. Since photodissociation of alkanes excited to these Rydberg states yields ground state products, an avoided crossing between an initially excited Rydberg state and a dissociative valence state must take place.[35]

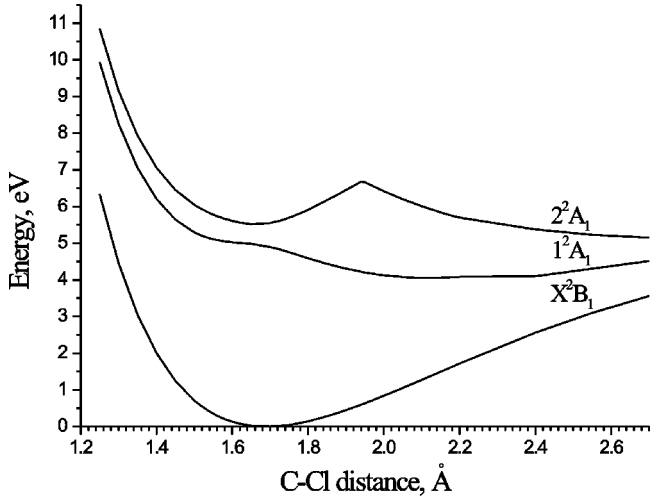

FIG. 2. Potential energy curves for the ground $X\,^2B_1$ and the two lowest $^2A_1$ excited states along the C–Cl coordinate (all other degrees of freedom are held at their ground state equilibrium values). All curves are shifted such that the ground state energy at equilibrium is zero.

Downloaded 14 Jul 2010 to 128.125.205.65. Redistribution subject to AIP license or copyright; see http://jcp.aip.org/jcp/copyright.jsp

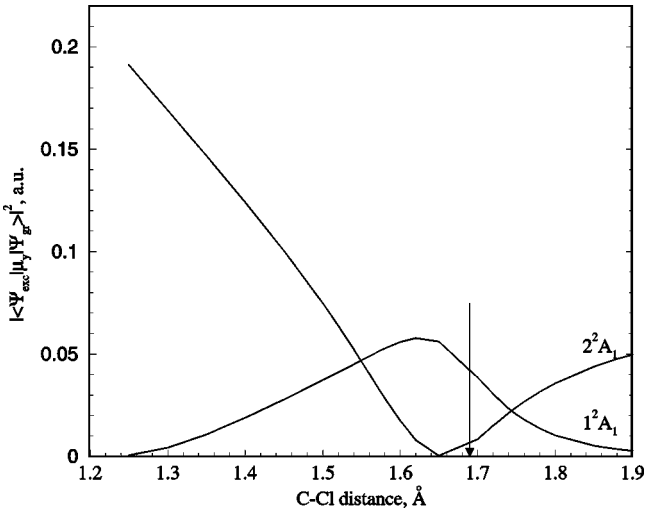

FIG. 3. Dipole strength dependence on the C–Cl distance for the $1\,^2A_1 \leftarrow X\,^2B_1$ and $2\,^2A_1 \leftarrow X\,^2B_1$ transitions. The vertical arrow indicates the ground state equilibrium C–Cl distance.

Salem[9] characterized avoided crossings due to Rydberg–valence interaction as avoided crossing between the relevant molecular orbitals (i.e., one-electron states). For open-shell species (like CH_2Cl), in which there are low-lying valence *and* Rydberg excited states derived from the promotion of the unpaired electron, this type of avoided crossing is expected to be quite common.

Obviously, the distinction between Rydberg and valence states is merely qualitative. From a quantum chemical perspective, an excited state is a Rydberg state if its configurational expansion is dominated by configurations in which the excited electron occupies diffuse (Rydberg) orbitals. We use this and several other criteria when assigning Rydberg or valence character to the excited states of CH_2Cl.[4] In this study, the size and spatial asymmetry of electron density are used.[42] Near the ground state equilibrium geometry, the $1\,^2A_1$ and $2\,^2A_1$ states can be assigned valence and $3s$ Rydberg character, respectively.[4] Changes in the size and asymmetry of the electron density along the C–Cl stretch reflect changes in the excited states' characters.

Figure 4(a) presents the spherical average $\langle r^2\rangle = \frac{1}{3}(\langle x^2\rangle + \langle y^2\rangle + \langle z^2\rangle)$ of the electron charge distribution for the ground and the two lowest excited states as a function of the carbon–chlorine separation. The monotonous increase of $\langle r^2\rangle$ for the ground state as the C–Cl distance increases reflects the increase in molecular size due to the C–Cl bond elongation. Therefore, it is convenient to eliminate this dependence by subtracting the ground state $\langle r^2\rangle$ from the $\langle r^2\rangle$ of the excited states. As can be seen in Fig. 4(b), the relative size of the electron charge distribution $\Delta\langle r^2\rangle$ of the $1\,^2A_1$ state is small at large C–Cl distances ($r_{CCl} \sim 1.8$ Å), then increases at smaller r_{CCl}, and remains approximately constant at $r_{CCl} < 1.56$ Å. $\Delta\langle r^2\rangle$ of the $2\,^2A_1$ state is larger than that of the $1\,^2A_1$ state at large r_{CCl}, then the difference between their relative sizes decreases as the C–Cl bond contracts, and it vanishes at $r_{CCl} = 1.62$ Å. This variation reflects the interaction between the two states. At shorter C–Cl distances, $\Delta\langle r^2\rangle$ of the $2\,^2A_1$ state continues to increase until it approaches a higher constant value at $r_{CCl} < 1.2$ Å.

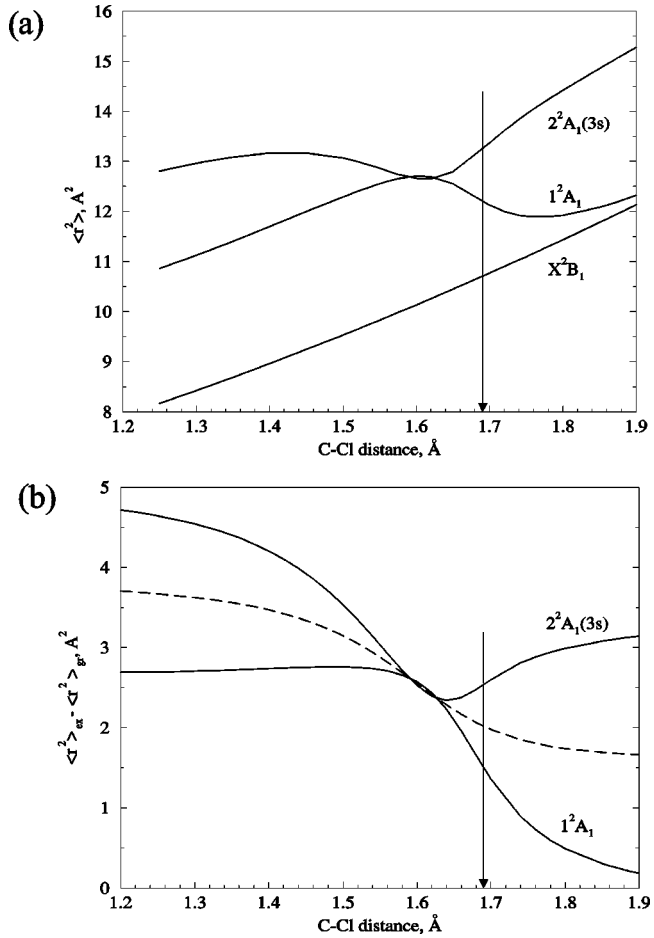

FIG. 4. Spherical average of the electron density, $\langle r^2\rangle$, as a function of the C–Cl distance for the ground and the two lowest $^2A_1$ excited states of the CH_2Cl radical (upper panel). The lower panel shows changes in the excited state density relative to the ground state, i.e., $\Delta\langle r^2\rangle = \langle r^2\rangle_{ex} - \langle r^2\rangle_{gr}$ (this subtracts changes due to molecular size increase at larger molecular separations). The dashed line corresponds to the average value for both states. The vertical arrow indicates the ground state equilibrium C–Cl distance.

This behavior confirms that the $1\,^2A_1$ and $2\,^2A_1$ states indeed interact with each other. However, the sum of $\Delta\langle r^2\rangle$ for these two states, which exchange their character, is not constant [the dashed line in Fig. 4(b) represents the average]. This implies that other states are mixed in. The increase in $\Delta\langle r^2\rangle$ of the $2\,^2A_1$ state at $r_{CCl} < 1.62$ Å signifies a higher Rydberg character. We identify this character as $3p_z$, based on the following observations. First, the next vertically excited state of A_1 symmetry above $2\,^2A_1$ is the Rydberg $3p_z$ state.[4] Second, the dipole strength of the transition to this state is the largest among the other calculated A_1 states, which explains the sharp rise of the dipole strength of the transition to the $2\,^2A_1$ state at small r_{CCl} (Fig. 3). Third, the calculated relative sizes of the electron density along the X, Y, and Z axes (presented in Fig. 5) demonstrate that the anisotropy of the $2\,^2A_1$ density increases and becomes much larger than that of the $1\,^2A_1$ state due to elongation of the electron density along the molecular axis (Z) as the C–Cl bond contracts. This indicates that the $2\,^2A_1$ state acquires Rydberg $3p_z$ character at short C–Cl distances.

Downloaded 14 Jul 2010 to 128.125.205.65. Redistribution subject to AIP license or copyright; see http://jcp.aip.org/jcp/copyright.jsp

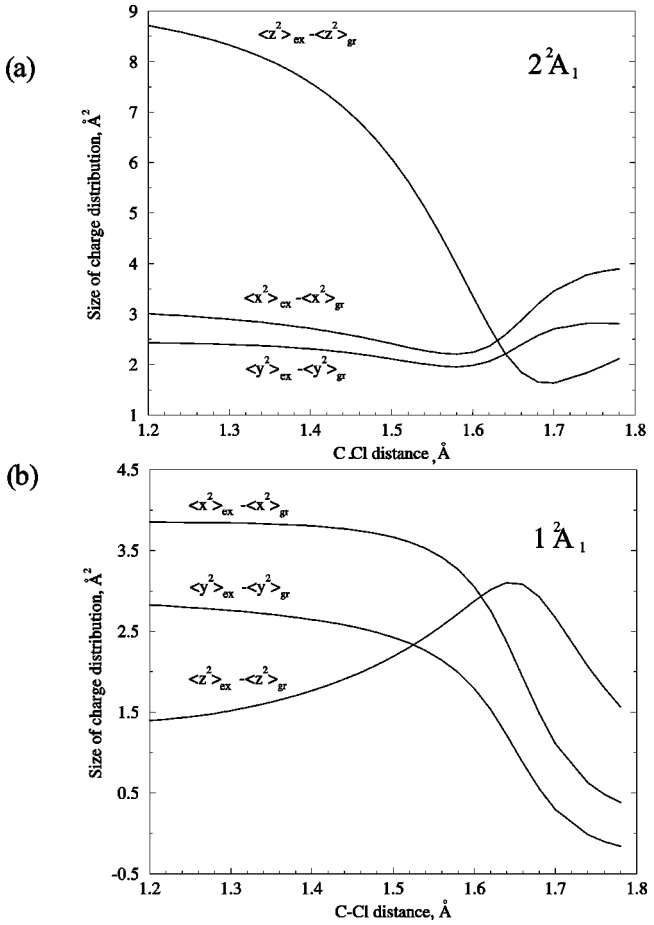

FIG. 5. $\langle x^2\rangle$, $\langle y^2\rangle$, and $\langle z^2\rangle$ components of the total electron charge distribution for $2\,^2A_1$ (upper panel) and $1\,^2A_1$ (lower panel) as a function of the C–Cl bond length. The molecular plane is the XZ plane, the C–Cl bond defines the Z axis.

The above analysis explains the interactions in the low-lying excited states of CH_2Cl, which are reflected in Fig. 4. At large C–Cl separations ($\sim$1.8 Å) the lowest excited state is the valence state derived from the $\sigma^* \leftarrow \pi^*$ excitation, while the second excited state has a predominant $3s$ character. At the ground state geometry ($\sim$1.69 Å) the two states are already mixed, but still retain their identities. At shorter C–Cl bond lengths ($<$1.6 Å), the lower state becomes the $3s$ Rydberg state, while the upper state acquires a mixed valence and Rydberg $3p_z$ character. The interaction with the $3p_z$ state leads to the double crossing of the curves in Fig. 4, and to the larger size of electron density for $2\,^2A_1$ at small r_{CCl}.

IV. ENHANCEMENT OF HOT BANDS' INTENSITIES

Based on the results of the *ab initio* calculations we can give now (at least qualitatively) an explanation for the ''hot bands'' enhancement in the absorption probability for the perpendicular $1\,^2A_1 \leftarrow X\,^2B_1$ transition. The probability of a transition between two states, which are characterized by the total wave functions $\Psi^0(\vec{r}_e,\vec{r}_N)$ and $\Psi^1(\vec{r}_e,\vec{r}_N)$ is proportional to the square of the transition dipole moment,

$$P \sim \left[\int \Psi^0(\vec{r}_e,\vec{r}_N)\vec{\mu}(\vec{r}_e)\Psi^1(\vec{r}_e,\vec{r}_N)dr \right]^2, \tag{4}$$

where $\vec{\mu}$ is the dipole moment operator, and $\vec{r}_e$ and $\vec{r}_N$ represent electronic and nuclear coordinates, respectively. In the Born–Oppenheimer approximation, $\Psi^0(\vec{r}_e,\vec{r}_N)$ and $\Psi^1(\vec{r}_e,\vec{r}_N)$ are separable into electronic and nuclear parts,

$$\Psi^i \approx \psi_e^i(\vec{r}_e;\vec{r}_N)\phi_{\mathrm{vib}}^i(\vec{r}_N), \quad i=0,1, \tag{5}$$

where $\phi_{\mathrm{vib}}^0(\vec{r}_N)$ and $\phi_{\mathrm{vib}}^1(\vec{r}_N)$ are vibrational functions for the initial and final electronic states, respectively, and the dependence of $\psi_e^i(\vec{r}_e;\vec{r}_N)$ on nuclear coordinates is parametric rather than explicit. Since $\phi_{\mathrm{vib}}^0(\vec{r}_N)$ and $\phi_{\mathrm{vib}}^1(\vec{r}_N)$ do not depend on electronic coordinates, Eq. (4) can be rewritten as

$$P \sim \left[\int \phi_{\mathrm{vib}}^0(\vec{r}_N)\vec{\mu}_e(\vec{r}_N)\phi_{\mathrm{vib}}^1(\vec{r}_N)d\vec{r}_N \right]^2, \tag{6}$$

where $\vec{\mu}_e(\vec{r}_N)$ is the electronic transition dipole moment, which is given by integration over the electronic coordinates $\vec{r}_e$,

$$\vec{\mu}_e(\vec{r}_N) = \int \psi_e^0(\vec{r}_e;\vec{r}_N)\vec{\mu}(\vec{r}_e)\psi_e^1(\vec{r}_e;\vec{r}_N)d\vec{r}_e. \tag{7}$$

As follows from Eq. (6), two factors contribute to the transition probability: the spatial overlap of the initial and final vibrational functions and the value of the electronic transition dipole moment in the region of maximum spatial overlap. For convenience, we discuss the dependence of the integral in Eq. (6) on vibrational excitation in terms of vibrational Franck–Condon factors and electronic transition dipole moments, although in our simulations we do not assume constant $\mu_e(R)$.

Although Eq. (6) should be integrated over all nuclear coordinates, because the transition to the $1\,^2A_1$ state mainly affects the C–Cl bond length we limit our qualitative treatment to a one-dimensional potential energy curve,

$$P \sim \left[\int_0^\infty \phi_{\mathrm{vib}}^0(R)\vec{\mu}_e(R)\phi_{\mathrm{vib}}^1(R)dR \right]^2, \tag{8}$$

where $\vec{\mu}_e(R)$ is the electronic transition dipole moment as a function of the C–Cl distance R. The lower state vibrational functions can be calculated either in the harmonic or (more accurately) in the Morse potential approximation. Since excitation occurs close to the dissociation threshold of the upper state, the corresponding wave function can be calculated in the linear approximation by using Airy functions.[43] The important feature of this wave function is that it is concentrated around the ''classical'' turning point and oscillates beyond this region, as shown schematically in Fig. 6. As a consequence, the vertical electronic transition is centered mostly near this turning point.

We were able to simulate qualitatively the enhanced probability for ''hot band'' excitation by calculating the Franck–Condon integrals for the ground and $1\,^2A_1$ states for Morse and Airy wave functions, respectively. This was done for the same range of photon energies as used in the experiments. By shifting the excited-state curve within the error

Downloaded 14 Jul 2010 to 128.125.205.65. Redistribution subject to AIP license or copyright; see http://jcp.aip.org/jcp/copyright.jsp

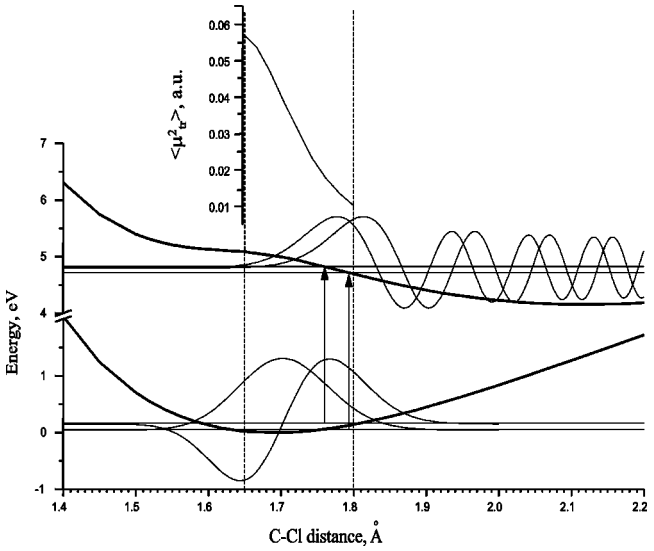

FIG. 6. Illustration of the hot bands' enhancement mechanism. Horizontal lines at the bottom of the potential energy curve for the ground state represent vibrational levels of the C–Cl stretch. Vertical arrows show electronic excitation upon absorption of a 266 nm photon. Transition dipole strength is shown in the inset.

bars of the calculations (± 0.1 eV; ± 0.1 Å), we could find conditions that gave enhancements that are comparable to the observed ones.

The simulations and the discussion above can now be combined to give a physical interpretation to the observed enhancement. The picture that emerges is illustrated in Fig. 6. The horizontal lines at the bottom of the ground state potential energy curve represent the ground and first excited vibrational levels of the C–Cl stretch. The vertical lines illustrate 266 nm absorption that promotes the radical to the excited $1\,^2A_1$ state. In the upper panel, the dipole strength of this transition is shown in the active Franck–Condon region (between the vertical dashed lines). As seen in Fig. 6, the spatial overlap of the vibrational functions in the ground and $1\,^2A_1$ states is small as a result of their very different equilibrium geometries.

At the low-energy edge of the perpendicular absorption band, the turning points on the $1\,^2A_1$ state are reached only at long C–Cl distances in the ground electronic state, where the probability density of the ground vibrational level is very small. Moreover, at these long C–Cl distances, the electronic transition strength is also small. This makes P small for excitation from the ground vibrational state.

Upon vibrational excitation in the ground electronic state, the probability density of the higher vibrational level is larger at long R than for the ground vibrational state. At long wavelengths, two effects conspire to enhance the absorption probability from excited vibrational states. First, the probability densities of the higher vibrational levels at long C–Cl distances are larger than for the ground vibrational state. This increases the vibrational Franck–Condon factor. Second, photon absorption originating in an excited vibrational level reaches the turning point on the upper electronic curve at shorter C–Cl distances. This increases not only the vibrational Franck–Condon overlap, but also the electronic dipole strength (see Fig. 6). The result is a significant increase in absorption probability for the "hot bands."

The enhancement effect is expected to be largest at the longest wavelengths. At shorter wavelengths the upper curve can be reached from the ground vibrational state at the equilibrium C–Cl distance, and therefore the contribution of the ground vibrational level will start to dominate. This agrees with the experimental observations.

V. CONCLUSIONS

This paper explains the enhancement in the electronic absorption probability for vibrationally excited CH_2Cl observed experimentally. For this purpose, we have calculated equilibrium structures, vibrational frequencies, and PESs for the ground, $X\,^2B_1$, and the two lowest excited states, $1\,^2A_1$ and $2\,^2A_1$, of CH_2Cl. We find that the changes in geometries and frequencies upon excitation are in good agreement with the molecular orbital picture developed in our previous work.[4] In order to estimate Franck–Condon factors, we have also calculated transition dipole moments for the $1\,^2A_1 \leftarrow X\,^2B_1$ and $2\,^2A_1 \leftarrow X\,^2B_1$ transitions.

Analysis of the size and asymmetry of the electron density at different C–Cl separations reveals that the valence $1\,^2A_1$ and the Rydberg $2\,^2A_1$ states exchange their character, which results in an avoided crossing at about 1.62 Å. This changes the shape of the $1\,^2A_1$ potential curve considerably. Moreover, a third Rydberg state is mixed in with the $2\,^2A_1$ state at shorter distances causing a significant increase in transition dipole strength.

These changes result in a large increase in Franck–Condon factors for absorption from vibrationally excited CH_2Cl. Our results demonstrate that the Rydberg–valence interactions, which have a pronounced effect on the photodynamics, involve more than two excited states of CH_2Cl, even within a small range of geometry variations. This confirms the importance and prevalence of Rydberg–valence interactions in open-shell systems.

ACKNOWLEDGMENTS

One of the authors (A.I.K.) gratefully acknowledges support from the National Science Foundation CAREER Award (Grant No. CHE-0094116), the Camille and Henry Dreyfus New Faculty Awards Program, the WISE Research Fund (USC), and the Donors of the Petroleum Research Fund administered by the American Chemical Society (PRF–AC). H.R. acknowledges support from the National Science Foundation (CHE-0209889).

[1] B.J. Finlayson-Pitts and J.N. Pitts, *Chemistry of the Upper and Lower Atmosphere: Theory, Experiments, and Applications* (Academic, New York, 1999).
[2] J.S. Francisco and M.M. Maricq, "Atmospheric photochemistry of alternative halocarbons," *Advances in Photochemistry* (Wiley, New York, 1995), Vol. 20, pp. 79–163.
[3] R. Schinke, *Photodissociation Dynamics*, Cambridge Monographs on Atomic, Molecular, and Chemical Physics (Cambridge University Press, Cambridge, 1993).
[4] S.V. Levchenko and A.I. Krylov, J. Chem. Phys. **115**, 7485 (2001).
[5] S.V. Levchenko and A.I. Krylov, J. Phys. Chem. A **106**, 5169 (2002).
[6] V. Dribinski, A.V. Demyanenko, A.B. Potter, and H. Reisler, J. Chem. Phys. **115**, 7474 (2001).

Downloaded 14 Jul 2010 to 128.125.205.65. Redistribution subject to AIP license or copyright; see http://jcp.aip.org/jcp/copyright.jsp

[7] A.B. Potter, V. Dribinski, A.V. Demyanenko, and H. Reisler, Chem. Phys. Lett. **349**, 257 (2001).
[8] P.B. Roussel, P.D. Lightfoot, F. Caraip, V. Catoire, R. Lesclaux, and W. Forst, J. Chem. Soc., Faraday Trans. **87**, 2367 (1991).
[9] L. Salem, Science **191**, 822 (1976).
[10] D.W. Kohn, H. Clauberg, and P. Chen, Rev. Sci. Instrum. **63**, 4003 (1992).
[11] A.V. Demyanenko, A.B. Potter, V. Dribinski, and H. Reisler, J. Chem. Phys. **117**, 2568 (2002).
[12] V. Dribinski, A. Ossadtchi, V.A. Mandelshtam, and H. Reisler, Rev. Sci. Instrum. **73**, 2634 (2002).
[13] S.G. Lias, J.E. Bartmess, J.F. Liebman, J.L. Holmes, R.D. Levin, and W.G. Mallard, J. Phys. Chem. Ref. Data **17**, 1 (1988).
[14] NIST Chemistry WebBook, webbook.nist.gov/chemistry/
[15] J.J. DeCorpo, D.A. Bafus, and J.L. Franklin, J. Chem. Thermodyn. **3**, 125 (1971).
[16] M. Weissman and S.W. Benson, J. Phys. Chem. **87**, 243 (1983).
[17] E. Tschuikow-Roux and S. Paddison, Int. J. Chem. Kinet. **19**, 15 (1987).
[18] J.L. Holmes and F.P. Lossing, J. Am. Chem. Soc. **110**, 7343 (1988).
[19] J.A. Seetula, J. Chem. Soc., Faraday Trans. **92**, 3069 (1996).
[20] J.A. Seetula, Phys. Chem. Chem. Phys. **2**, 3807 (2000).
[21] K. Mikhaylichenko, C. Riehn, L. Valachovic, A. Sanov, and C. Wittig, J. Chem. Phys. **105**, 6807 (1996).
[22] M.R. Cameron and S.H. Kable, Rev. Sci. Instrum. **67**, 283 (1996).
[23] M.E. Jacox and D.E. Milligan, J. Chem. Phys. **53**, 2688 (1970).
[24] L. Andrews and D.W. Smith, J. Chem. Phys. **53**, 2956 (1970).
[25] K. Raghavachari, G.W. Trucks, J.A. Pople, and M. Head-Gordon, Chem. Phys. Lett. **157**, 479 (1989).
[26] J.F. Stanton, J. Gauss, J.D. Watts, W.J. Lauderdale, and R.J. Bartlett, ACES II, 1993. The package also contains modified versions of the MOLECULE Gaussian integral program of J. Almlöf and P.R. Taylor, the ABACUS integral derivative program written by T.U. Helgaker, H.J.Aa. Jensen, P. Jørgensen, and P.R. Taylor, and the PROPS property evaluation integral code of P.R. Taylor.
[27] H. Koch, H. Jørgen Aa. Jensen, and P. Jørgensen, J. Chem. Phys. **93**, 3345 (1990).
[28] J.F. Stanton and R.J. Bartlett, J. Chem. Phys. **98**, 7029 (1993).
[29] G.D. Purvis and R.J. Bartlett, J. Chem. Phys. **76**, 1910 (1982).
[30] R. Krishnan, J.S. Binkley, R. Seeger, and J.A. Pople, J. Chem. Phys. **72**, 650 (1980).
[31] A.D. McLean and G.S. Chandler, J. Chem. Phys. **72**, 5639 (1980).
[32] M.J. Frisch, J.A. Pople, and J.S. Binkley, J. Chem. Phys. **80**, 3265 (1984).
[33] T. Clark, J. Chandrasekhar, and P.V.R. Schleyer, J. Comput. Chem. **4**, 294 (1983).
[34] We also attempted to optimize the structure of the $2\ ^2A_1$ Rydberg state by using the EOM–CCSD method, however, because of the strong coupling between this state and the valence state we were unable to locate the equilibrium structure of the Rydberg state on the multidimensional PES.
[35] M.S. Gordon and J.W. Caldwell, ''Excited states of saturated molecules,'' in *Excited States in Organic Chemistry and Biochemistry*, edited by B. Pullman and N. Goldblum (Reidel, Dordrecht, Holland, 1977), pp. 257–270.
[36] J. Verges, C. Effantin, J. d'Incan, D.L. Cooper, and R.F. Barrow, Phys. Rev. Lett. **53**, 46 (1984).
[37] Ch. Meier and V. Engel, Chem. Phys. Lett. **212**, 691 (1993).
[38] Ch. Meier and V. Engel, J. Chem. Phys. **101**, 2673 (1994).
[39] Y. Arasaki, K. Takatsuka, K. Wang, and V. McKoy, J. Chem. Phys. **112**, 8871 (2000).
[40] D.D. Konowalow and J.L. Fish, Chem. Phys. **84**, 463 (1984).
[41] M.S. Gordon, Chem. Phys. Lett. **52**, 161 (1977).
[42] The size of electron density can be estimated as an expectation value of the one-electron operator $\frac{1}{3}(\hat{x}^2+\hat{y}^2+\hat{z}^2)$. By considering $\langle\hat{x}^2\rangle$, $\langle\hat{y}^2\rangle$, and $\langle\hat{z}^2\rangle$ separately one can characterize the deviation of the electron distribution from a spherical shape. For *s*-type Rydberg states this deviation is expected to be small, while *p*-type Rydberg states will exhibit larger charge anisotropy.
[43] L.D. Landau and E.M. Lifshitz, *Quantum Mechanics: Non-relativistic Theory* (Pergamon, Oxford, 1977).

Downloaded 14 Jul 2010 to 128.125.205.65. Redistribution subject to AIP license or copyright; see http://jcp.aip.org/jcp/copyright.jsp